GEOPHYSICS, VOL. 65, NO. 5 (SEPTEMBER-OCTOBER 2000); P. 1501–1513, 18 FIGS.

Electromagnetic inversion using quasi-linear approximation

Michael S. Zhdanov*, Sheng Fang‡, and Gábor Hursán*

ABSTRACT

Three-dimensional electromagnetic inversion continues to be a challenging problem in electrical exploration. We have recently developed a new approach to the solution of this problem based on quasi-linear approximation of a forward modeling operator. It generates a linear equation with respect to the modified conductivity tensor, which is proportional to the reflectivity tensor and the complex anomalous conductivity. We solved this linear equation by using the regularized conjugate gradient method. After determining a modified conductivity tensor, we used the electrical reflectivity tensor to evaluate the anomalous conductivity. Thus, the developed inversion scheme reduces the original nonlinear inverse problem to a set of linear inverse problems. The developed algorithm has been realized in computer code and tested on synthetic 3-D EM data. The case histories include interpretation of a 3-D magnetotelluric survey conducted in Hokkaido, Japan, and the 3-D inversion of the tensor controlled-source audio magnetotelluric data over the Sulphur Springs thermal area, Valles Caldera, New Mexico, U.S.A.

INTRODUCTION

During the last decade, considerable advances were made in developing a multidimensional electromagnetic (EM) interpretation technique. Several papers were published during this period on 3-D inversion of EM data (Eaton, 1989; Madden and Mackie, 1989; Smith and Booker, 1991; Lee and Xie, 1993; Oristaglio et al., 1993; Pellerin et al., 1993; Nekut, 1994; Zhdanov and Keller, 1994; Torres-Verdin and Habashy, 1995; Xie and Lee, 1995; Newman and Alumbaugh, 1996). However, the development of effective interpretation schemes for 3-D inhomogeneous geological structures is still one of the most challenging problems in EM geophysics.

In our recent publications (Zhdanov and Fang, 1996a, b), we developed a novel approach to 3-D EM forward modeling and inversion based on linearization of the integral equations for scattered EM fields. In this paper, we discuss a new development of this method using a regularized conjugate gradient inversion scheme, and we present the results of case history studies. For completeness, we also include an overview of the main principles of quasi-linear (QL) inversion.

The QL approximation is based on the assumption that the anomalous field $\mathbf{E}^a$ is linearly related to the normal (background) field $\mathbf{E}^b$ in the inhomogeneous domain: $\mathbf{E}^a = \hat{\lambda}\mathbf{E}^b$, where $\hat{\lambda}$ is an electrical reflectivity tensor which is a slowly varying function of position and frequency. In the inversion, we introduce a modified material property tensor $\hat{\mathbf{m}}$, proportional to the reflectivity tensor and the anomalous conductivity $\Delta\sigma$. In this case, the QL approximation generates a linear equation with respect to the modified material property tensor $\hat{\mathbf{m}}$. After determining $\hat{\mathbf{m}}$, we use the electrical reflectivity tensor $\hat{\lambda}$ to evaluate the anomalous conductivity $\Delta\sigma$.

The developed algorithm has been realized in the QLINV3D computer code and tested on synthetic 3-D EM data. Synthetic inversion examples, with and without random noise, have demonstrated that the algorithm for inverting 3-D EM data is fast and stable. The case histories presented here include interpretation of a 3-D magnetotelluric (MT) survey conducted by the New Energy and Industrial Technology Development Organization (NEDO) in the Minamikayabe area in the southern part of Hokkaido, Japan, and 3-D inversion of the tensor controlled-source audio magnetotelluric (CSAMT) data collected by Phil Wannamaker over the Sulphur Springs thermal area, Valles Caldera, New Mexico, U.S.A. The interpretation of real data demonstrates that the 3-D quasi-linear EM inversion can be a practical tool of geophysical EM data analysis.

QUASI-LINEAR INVERSION

Consider a 3-D geoelectric model with the normal (background) conductivity σ_b and local inhomogeneity D with an arbitrarily varying conductivity $\sigma = \sigma_b + \Delta\sigma$. The model is excited

Manuscript received by the Editor June 12, 1998; revised manuscript received January 24, 2000.
*University of Utah, Department of Geology and Geophysics, Salt Lake City, Utah 84112-0111. E-mail: mzhdanov@mines.utah.edu.
‡Formerly University of Utah, Department of Geology and Geophysics, Salt Lake City, Utah 84112-0111; presently Baker Atlas, 10201 Westheimer WA-IA, Houston, Texas. E-mail: Sheng.Fang@waii.com.

by an electromagnetic field generated by an arbitrary source. We consider a quasi-stationary model of the field, so we neglect the displacement currents as is usual in low frequency geophysical applications (Zhdanov and Keller, 1994). The electromagnetic fields in this model can be presented as a sum of the background and anomalous fields:

$$\mathbf{E} = \mathbf{E}^{\mathbf{b}} + \mathbf{E}^{\mathbf{a}}, \qquad \mathbf{H} = \mathbf{H}^{\mathbf{b}} + \mathbf{H}^{\mathbf{a}}, \tag{1}$$

where the background field is a field generated by the given sources in the model with the background distribution of conductivity σ_b, and the anomalous field is produced by the anomalous conductivity distribution $\Delta\sigma$.

It is well known that the anomalous field in the frequency domain can be presented as an integral over the excess currents in the inhomogeneous domain D (Weidelt, 1975):

$$\mathbf{F}^{\mathbf{a}}(\mathbf{r_j}) = \iiint_{\mathbf{D}} \hat{\mathbf{G}}^{\mathbf{F}}(\mathbf{r_j} \mid \mathbf{r})\Delta\sigma(\mathbf{r})[\mathbf{E}^{\mathbf{b}}(\mathbf{r}) + \mathbf{E}^{\mathbf{a}}(\mathbf{r})]\,\mathbf{dv}, \tag{2}$$

where $\mathbf{F}^{\mathbf{a}}$ stands for $\mathbf{E}^{\mathbf{a}}$ or $\mathbf{H}^{\mathbf{a}}$ observed on the surface of the earth, and $\hat{\mathbf{G}}^{F}(\mathbf{r_j} \mid \mathbf{r})$ stands for the electric or magnetic Green's tensor defined for an unbounded conductive medium with the normal conductivity σ_b.

We apply the quasi-linear approach (Zhdanov and Fang, 1996a, b),

$$\mathbf{E}^{\mathbf{a}}(\mathbf{r}) \approx \hat{\lambda}(\mathbf{r})\mathbf{E}^{\mathbf{b}}(\mathbf{r}), \tag{3}$$

to equation (2), which yields

$$\mathbf{F}^{\mathbf{a}} \approx \iiint_{\mathbf{D}} \hat{\mathbf{G}}^{\mathbf{F}}(\mathbf{r_j} \mid \mathbf{r})\Delta\sigma(\mathbf{r})[\hat{\mathbf{I}} + \hat{\lambda}(\mathbf{r})]\mathbf{E}^{\mathbf{b}}(\mathbf{r})\,\mathbf{dv}, \tag{4}$$

where $\hat{\lambda}$ is an electrical reflectivity tensor, and $\hat{\mathbf{I}}$ is the unit tensor.

We introduce a new tensor function

$$\hat{\mathbf{m}}(\mathbf{r}) = \Delta\sigma(\mathbf{r})[\hat{\mathbf{I}} + \hat{\lambda}(\mathbf{r})], \tag{5}$$

which we call *a modified material property tensor.* Equation (5) can be treated as a modification of Ohm's law:

$$\mathbf{j}^{\mathbf{D}} = \Delta\sigma\mathbf{E} = \Delta\sigma(\mathbf{E}^{\mathbf{b}} + \mathbf{E}^{\mathbf{a}}) = \Delta\sigma[\hat{\mathbf{I}} + \hat{\lambda}(\mathbf{r})]\mathbf{E}^{\mathbf{b}}. \tag{6}$$

The modified material property tensor can be considered as the ratio of the anomalous, induced currents, $\mathbf{j}^{\mathbf{D}}$, to the background electric field. Finally, equation (4) takes the form

$$\mathbf{F}^{\mathbf{a}}(\mathbf{r_j}) \approx \iiint_{\mathbf{D}} \hat{\mathbf{G}}^{\mathbf{F}}(\mathbf{r_j} \mid \mathbf{r})\hat{\mathbf{m}}(\mathbf{r})\mathbf{E}^{\mathbf{b}}(\mathbf{r})\mathbf{dv} = \mathbf{G}^{\mathbf{F}}(\hat{\mathbf{m}}), \tag{7}$$

where $\mathbf{G}^{\mathbf{F}}$ is the corresponding Green's linear operator.

The last equation is a linear one with respect to $\hat{\mathbf{m}}(\mathbf{r})$. In our algorithm, we adopt the regularized conjugate gradient method for determining the modified material property tensor (Zhdanov, 1993).

The reflectivity tensor $\hat{\lambda}$ can be determined from the following linear equation inside the inhomogeneous domain D, as long as we know $\hat{\mathbf{m}}$:

$$\begin{aligned}\mathbf{E}^{\mathbf{a}}(\mathbf{r_j}) &\approx \iiint_{\mathbf{D}} \hat{\mathbf{G}}^{\mathbf{E}}(\mathbf{r_j} \mid \mathbf{r})\hat{\mathbf{m}}(\mathbf{r})\mathbf{E}^{\mathbf{b}}(\mathbf{r})\,\mathbf{dv} \\ &\approx \hat{\lambda}(\mathbf{r_j})\mathbf{E}^{\mathbf{b}}(\mathbf{r_j}).\end{aligned} \tag{8}$$

After determining $\hat{\mathbf{m}}$ and $\hat{\lambda}$, it is possible to evaluate the anomalous conductivity distribution $\Delta\sigma$ from equation (5).

This inversion scheme reduces the original nonlinear inverse problem to three linear inverse problems: the first one (the quasi-Born inversion) for the parameter $\hat{\mathbf{m}}$, another one for the parameter $\hat{\lambda}$, and the third one (a correction of the result of the quasi-Born inversion) for the conductivity $\Delta\sigma$. It is based on a QL approximation; that is why we call this approach *a QL inversion.*

Note that we can rewrite equation (7) using matrix notations:

$$\mathbf{F} = \mathbf{G}^{\mathbf{F}}\mathbf{m}. \tag{9}$$

Here $\mathbf{m}$ is the vector-column of the modified conductivity tensor $\hat{\mathbf{m}}$, $\mathbf{F}$ is the vector-column of the data, and the matrix $\mathbf{G}^{\mathbf{F}}$ is the matrix of the linear Green's operator defined by formula (7).

Similarly, we can get from (8)

$$\lambda\mathbf{E}^{\mathbf{b}} = \mathbf{G}^{\mathbf{E}}\mathbf{m}, \tag{10}$$

where λ is a block-diagonal matrix of reflectivity tensors, $\mathbf{E}^{\mathbf{b}}$ is the vector-column of the background field, and $\mathbf{G}^{\mathbf{E}}$ denotes a matrix of linear operators defined by expression (7) with the electric Green's tensor. Equation (5) in matrix notations takes the form

$$\mathbf{m} = \boldsymbol{\Delta}\sigma[\mathbf{I} + \lambda], \tag{11}$$

where $\mathbf{I}$ is the unit matrix.

The solution of the inverse problem is reduced to the inversion of linear system (9) with respect to $\mathbf{m}$ and then to the inversion of equation (10) with respect to λ. After that, we obtain $\boldsymbol{\Delta}\sigma$ using equation (11). We apply the Tikhonov regularization theory to solve this system of linear equations (Tikhonov and Arsenin, 1977).

THE REGULARIZED CONJUGATE GRADIENT METHOD FOR SOLVING LINEAR INVERSE PROBLEM EQUATIONS

Note that the solution of equation (7) and, correspondingly, equation (9) can be nonunique in the general case since there may exist $\hat{\mathbf{m}}(\mathbf{r})$ distributions that produce a zero external field, similar to the existence of the current distributions producing zero external field (Habashy et al., 1994; Svetov and Gubatenko, 1985). However, according to the uniqueness theorem by Gusarov (1981) the excess conductivity $\Delta\sigma(\mathbf{r})$ can be found uniquely in the class of piecewise-analytic functions. Therefore, to make our solution unique, we have to develop a unified approach for simultaneously finding $\hat{\mathbf{m}}$, $\hat{\lambda}$, and $\Delta\sigma$.

We use the method of constrained inversion developed by Zhdanov and Chernyak (1987). A similar approach to 2-D inverse scattering problems was discussed also by Kleinman and van den Berg (1993). It is based on the introduction of the parametric functional

$$P^{\alpha}(\mathbf{m}) = \phi(\mathbf{m}) + \alpha\,\mathbf{S}(\mathbf{m}), \tag{12}$$

where the misfit functional is specified as

$$\phi(\mathbf{m}) = \|\mathbf{G}^{\mathbf{F}}\mathbf{m} - \mathbf{F}\|^2 + \|\mathbf{m} - \boldsymbol{\Delta}\sigma(\mathbf{I} + \lambda)\|^2, \tag{13}$$

and the stabilizer is selected to be equal to

$$S(\mathbf{m}) = \|\mathbf{m} - \mathbf{m}_{\mathbf{apr}}\|^2. \tag{14}$$

The a priori model $\mathbf{m}_{\mathbf{apr}}$ is some reference model, selected on the basis of all available geological and geophysical information about the area under investigation. The scalar multiplier α is a regularization parameter.

As one can see from equation (13), the misfit functional takes care not only of the solution of equation (9) but, simultaneously, also fulfilling of the modified Ohm's law (5).

Now, the inversion is reduced to the solution of the minimization problem for the parametric functional:

$$P^{\alpha}(\mathbf{m}) = \min. \tag{15}$$

One can calculate the first variation of the parametric functional under the assumption that $\Delta\sigma$ and λ are, temporarily, constants:

$$\delta P^{\alpha}(\mathbf{m}) = 2\mathrm{Re}\{\delta\mathbf{m}^*[\mathbf{G}^{\mathbf{F}*}(\mathbf{G}^{\mathbf{F}}\mathbf{m} - \mathbf{F}) + (\mathbf{m} - \Delta\sigma[\mathbf{I} + \lambda]) + \alpha(\mathbf{m} - \mathbf{m}_{\mathbf{apr}})]\},$$

where the asterisk "*" denotes transposed complex conjugate matrices.

Let us select $\delta\mathbf{m}$ as

$$\delta\mathbf{m} = -k\mathbf{l}^{\alpha}(\mathbf{m}), \qquad 0 < k < \infty, \tag{16}$$

where

$$\mathbf{l}^{\alpha}(\mathbf{m}) = \mathbf{G}^{\mathbf{F}*}(\mathbf{G}^{\mathbf{F}}\mathbf{m} - \mathbf{F}) + (\mathbf{m} - \Delta\sigma[\mathbf{I} + \lambda]) + \alpha(\mathbf{m} - \mathbf{m}_{\mathbf{apr}}), \tag{17}$$

and k is the length of the iteration step.

This selection makes $\delta P^{\alpha}(\mathbf{m}) = -2k^{\alpha}\mathrm{Re}\{\mathbf{l}^{\alpha*}(\mathbf{m})\mathbf{l}^{\alpha}(\mathbf{m})\} < 0$. That means that the parametric functional is reduced if we apply perturbation (16) to the model parameters.

In order to accelerate the convergence, we apply the regularized conjugate gradient method described by the following iteration process:

$$\mathbf{m}_{\mathbf{n}+1} = \mathbf{m}_{\mathbf{n}} + \delta\mathbf{m}_{\mathbf{n}} = \mathbf{m}_{\mathbf{n}} - k_{\mathbf{n}}\tilde{\mathbf{l}}^{\alpha}(\mathbf{m}_{\mathbf{n}}),$$

where the "directions" of ascent $\tilde{\mathbf{l}}^{\alpha}(\mathbf{m}_{\mathbf{n}})$ are selected according to the algorithm described below.

In the first step, we use the "direction" of regularized steepest ascent determined by equation (17):

$$\tilde{\mathbf{l}}^{\alpha}(\mathbf{m}_0) = \mathbf{l}^{\alpha}(\mathbf{m}_0).$$

Therefore, the first iteration is computed by the formula

$$\mathbf{m}_1 = \mathbf{m}_0 + \delta\mathbf{m}_0 = \mathbf{m}_0 - k_0\left[\mathbf{G}^{\mathbf{F}*}(\mathbf{G}^{\mathbf{F}}\mathbf{m}_{\mathbf{apr}} - \mathbf{F})\right], \tag{18}$$

where

$$\mathbf{m}_{\mathbf{apr}} = \Delta\sigma_{\mathbf{apr}}[\mathbf{I} + \lambda_{\mathbf{apr}}],$$

and $\Delta\sigma_{\mathbf{apr}}$ and $\lambda_{\mathbf{apr}}$ are the parameters of the reference model.

The second iteration is

$$\mathbf{m}_2 = \mathbf{m}_1 + \delta\mathbf{m}_1 = \mathbf{m}_1 - k_1\tilde{\mathbf{l}}^{\alpha}(\mathbf{m}_1), \tag{19}$$

where

$$\tilde{\mathbf{l}}^{\alpha}(\mathbf{m}_1) = \mathbf{l}^{\alpha}(\mathbf{m}_1) + \beta_1\tilde{\mathbf{l}}^{\alpha}(\mathbf{m}_0)$$

and

$$\mathbf{l}^{\alpha}(\mathbf{m}_1) = \mathbf{G}^{\mathbf{F}*}(\mathbf{G}^{\mathbf{F}}\mathbf{m}_1 - \mathbf{F}) + (\mathbf{m}_1 - \Delta\sigma_{\mathbf{apr}}[\mathbf{I} + \lambda_1]) + \alpha(\mathbf{m}_1 - \mathbf{m}_{\mathbf{apr}}). \tag{20}$$

On the $(n+1)$th step

$$\mathbf{m}_{\mathbf{n}+1} = \mathbf{m}_{\mathbf{n}} + \delta\mathbf{m}_{\mathbf{n}} = \mathbf{m}_{\mathbf{n}} - k_{\mathbf{n}}\tilde{\mathbf{l}}^{\alpha}(\mathbf{m}_{\mathbf{n}}), \tag{21}$$

and

$$\tilde{\mathbf{l}}^{\alpha}(\mathbf{m}_{\mathbf{n}}) = \mathbf{l}^{\alpha}(\mathbf{m}_{\mathbf{n}}) + \beta_{\mathbf{n}}\tilde{\mathbf{l}}^{\alpha}(\mathbf{m}_{\mathbf{n}-1}),$$

where

$$\mathbf{l}^{\alpha}(\mathbf{m}_{\mathbf{n}}) = \mathbf{G}^{\mathbf{F}*}(\mathbf{G}^{\mathbf{F}}\mathbf{m}_{\mathbf{n}} - \mathbf{F}) + (\mathbf{m}_{\mathbf{n}} - \Delta\sigma_{\mathbf{n}-1}[\mathbf{I} + \lambda_{\mathbf{n}}]) + \alpha(\mathbf{m}_{\mathbf{n}} - \mathbf{m}_{\mathbf{apr}}). \tag{22}$$

The matrix of the reflectivity tensor $\lambda_{\mathbf{n}}$ is determined from the matrix $\mathbf{m}_{\mathbf{n}}$ using equation (10):

$$\lambda_{\mathbf{n}}\mathbf{E}^{\mathbf{b}} = \mathbf{G}^{\mathbf{E}}\mathbf{m}_{\mathbf{n}}. \tag{23}$$

The anomalous conductivity on the $(n-1)$th iteration can be found using equation (11). Note that the anomalous conductivity has to satisfy the condition

$$\Delta\sigma_{\mathbf{n}-1} > -\sigma_{\mathbf{b}}, \tag{24}$$

because the electrical conductivity has to be positive. Notice also that equation (11) should hold for any frequency. In reality, of course, it holds only approximately. Therefore the conductivity $\Delta\sigma_{\mathbf{n}-1}$ can be found by using the least-squares method of solving equation (11):

$$\Delta\sigma_{\mathbf{n}-1} = \mathrm{Re}\left(\sum_{\omega}\mathbf{m}_{\mathbf{n}-1}(\mathbf{I} + \lambda_{\mathbf{n}-1})^*\right) \times \left[\sum_{\omega}[(\mathbf{I} + \lambda_{\mathbf{n}-1})^*(\mathbf{I} + \lambda_{\mathbf{n}-1})]\right]^{-1} = \mathbf{a}_{\mathbf{n}-1}, \quad \text{for } \mathbf{a}_{\mathbf{n}-1} > -\sigma_{\mathbf{b}}, \tag{25}$$

and

$$\Delta\sigma_{\mathbf{n}-1} = -\frac{1}{2}\sigma_{\mathbf{b}} \quad \text{for } \mathbf{a}_{\mathbf{n}-1} \le -\sigma_{\mathbf{b}}. \tag{26}$$

The coefficient k_n can be determined from the condition

$$P^{\alpha}(\mathbf{m}_{\mathbf{n}+1}) = \mathbf{P}^{\alpha}(\mathbf{m}_{\mathbf{n}} - k_{\mathbf{n}}\tilde{\mathbf{l}}^{\alpha}(\mathbf{m}_{\mathbf{n}})) = \mathbf{f}(k_{\mathbf{n}}) = \min.$$

Solution of this minimization problem gives the following best estimate for the length of the step:

$$k_n = \frac{\tilde{\mathbf{l}}^{\alpha*}(\mathbf{m}_{\mathbf{n}})\mathbf{l}^{\alpha}(\mathbf{m}_{\mathbf{n}})}{\tilde{\mathbf{l}}^{\alpha*}(\mathbf{m}_{\mathbf{n}})(\mathbf{G}^{\mathbf{F}*}\mathbf{G}^{\mathbf{F}} + \alpha\mathbf{I})\tilde{\mathbf{l}}^{\alpha}(\mathbf{m}_{\mathbf{n}})}. \tag{27}$$

The conjugate gradient method requires that the vectors $\tilde{\mathbf{l}}^{\alpha}(\mathbf{m}_{\mathbf{n}})$ will be mutually conjugate. This requirement is fulfilled if the coefficients β_n are determined by the formula (Tarantola, 1987):

$$\beta_n = \frac{\left\|\mathbf{l}^{\alpha}(\mathbf{m}_{\mathbf{n}})\right\|^2}{\left\|\mathbf{l}^{\alpha}(\mathbf{m}_{\mathbf{n}-1})\right\|^2}.$$

Using equations (17), (18), and (27), we can obtain $\mathbf{m}$ iteratively.

The regularization parameter α describes the trade-off between the best fitting and reasonable stabilization. In a case where α is selected as too small, the minimization of the parametric functional $P^{\alpha}(\mathbf{m})$ is equivalent to the minimization of the misfit functional $\phi(\mathbf{m})$. Therefore we have no regularization, which can result in an unstable incorrect solution. When α is too large, the minimization of the parametric functional $P^{\alpha}(\mathbf{m})$ is equivalent to the minimization of the stabilizing functional $S(\mathbf{m})$, which will force the solution to be closer to the a priori model. Ultimately, we would expect the final model to be exactly like the a priori model, while the observed data are totally ignored in the inversion. Thus, the critical question in the regularized solution of the inverse problem is the selection of the optimal regularization parameter α. The basic principles used for determining the regularization parameter α are discussed by Tikhonov and Arsenin (1977) and Zhdanov and Keller (1994).

The traditional numerical method to determine the parameter α is based on the following simple idea. Consider for example the progression of numbers

$$\alpha_k = \alpha_0 q^k; \qquad k = 0, 1, 2, \ldots, n; \quad q > 0. \tag{28}$$

For any number α_k we can find an element $\mathbf{m}_{\alpha_k}$, minimizing $P^{\alpha_k}(\mathbf{m})$, and calculate the misfit $\|\mathbf{G}^{\mathbf{F}}\mathbf{m}_{\alpha_k} - \mathbf{F}\|^2$. The optimal value of the parameter α is the number α_{k0}, for which we have

$$\left\| \mathbf{G}^{\mathbf{F}}\mathbf{m}_{\alpha_{k0}} - \mathbf{F} \right\|^2 = \delta, \tag{29}$$

where δ is the level of noise in observed data. Equality (29) is called *the misfit condition.*

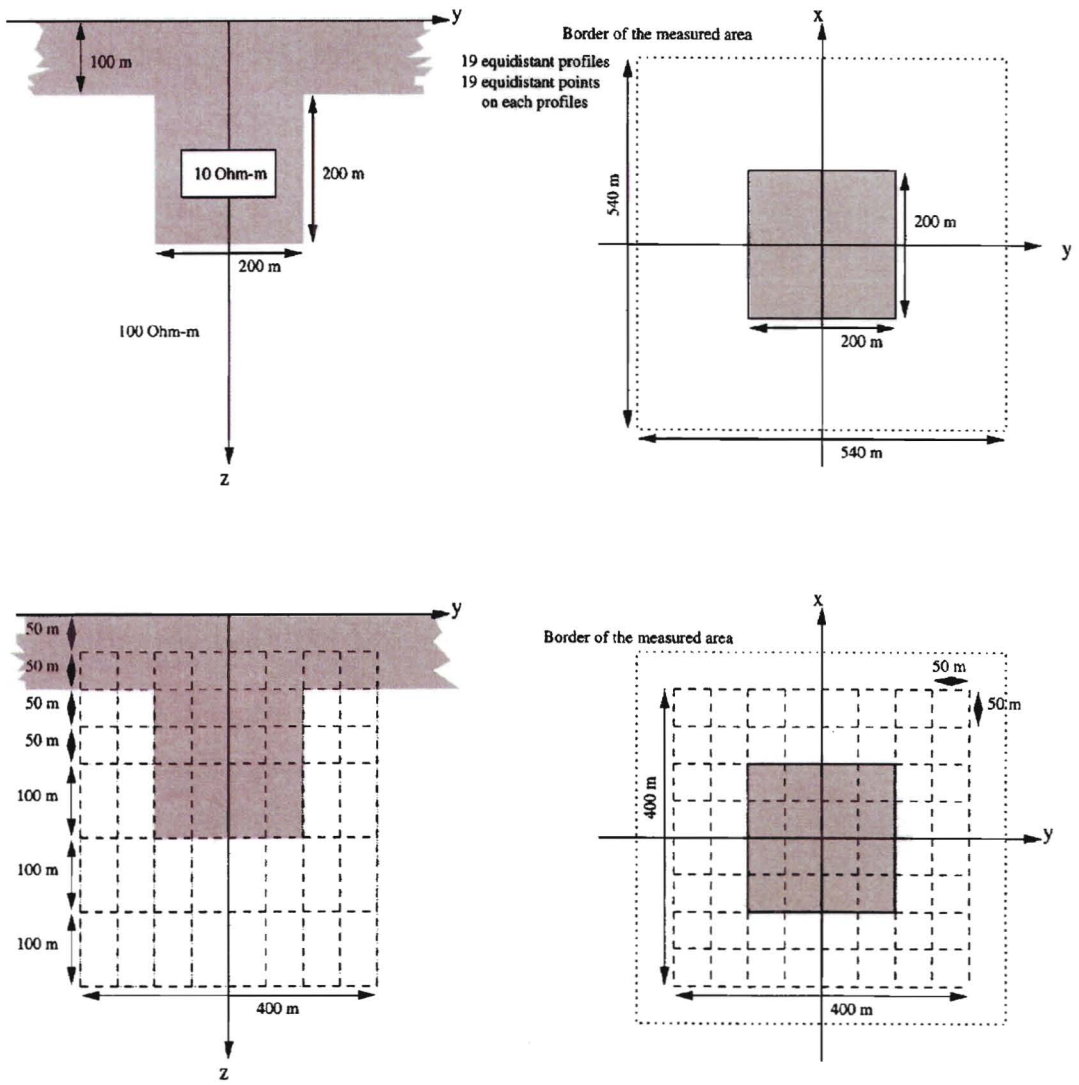

FIG. 1. 3-D model of a synclinal structure in the near-surface conductive layer excited by a plane wave, and its subdivision into cells used for the inversion.

In our code, we use the following algorithm of the regularized conjugate gradient method:

$$\tilde{\mathbf{I}}^{\alpha_{n+1}}(\mathbf{m}_{n+1}) = \mathbf{I}^{\alpha_{n+1}}(\mathbf{m}_{n+1}) + \beta_{n+1}\tilde{\mathbf{I}}^{\alpha_n}(\mathbf{m}_n),$$

where α_n are the subsequent values of the regularization parameter. This method is called the *adaptive* regularization method (Tikhonov and Arsenin, 1977). In order to avoid divergence, we begin an iteration from a big value of α (e.g., $\alpha_0 = 10\,000.$), then reduce α_n ($\alpha_n = \alpha_{n-1}/2$) on each subsequent iteration, and continuously iterate until the misfit condition (29) is reached.

MODEL STUDY OF 3-D QUASI-LINEAR INVERSION METHOD

The method was carefully tested on a number of 3-D models describing different typical geoelectrical situations. We will present here just one example of the model study.

The model represents a synclinal structure in the near-surface conductive layer with 10 ohm-m resistivity. The horizontal and vertical cross-sections of the model are shown in Figure 1. The model was excited by a plane EM wave. The theoretical observed field was calculated at the nodes of a square grid on the surface using the integral equation (IE) forward modeling code SYSEM (Xiong, 1992). The distance between the observation points is 30 m in the X and Y directions.

Following the traditional approach used in practical MT observations, we calculated synthetic observed apparent resistivities and phases based on two off-diagonal elements of the magnetotelluric tensor at each observation point. The quantities ρ_{yx} and ϕ_{yx} are assigned to the nominal TE mode, whereas ρ_{xy} and ϕ_{xy} are assigned to the nominal TM mode. Note that this 2-D nomenclature is artificial and approximate in nature for 3-D structures. However, it is widely used in practical MT observations, and usually only the quantities ρ_{yx}, ϕ_{yx}, ρ_{xy}, and ϕ_{xy} are available for inversion. That is why we use the same approach in the model study.

Magnetotelluric apparent resistivities and phases were calculated for the frequencies f = 0.5, 1, 2, 5, 10, 20, 50, 100, 200, and 500 Hz. Thus the synthetic MT data set which we use for inversion corresponds to 361 observation points and 10 frequencies. As an example, the synthetic observed magnetotelluric sounding curves at a point ($x = 0$, $y = 90$ m) are shown in Figure 2 by solid lines.

We defined an inverse area as a rectangular body with sides of 400 m in both horizontal directions and of 450 m in a vertical direction. It was divided into rectangular cells with constant but unknown resistivities. The boundaries of the cells used for inversion are shown by dashed lines in Figure 1.

We applied QL inversion simultaneously to TE and TM data with 3% random noise added. We used the adaptive scheme described above for selecting the optimum regularization parameter α. The initial value of α_0 was reduced in the process of conjugate gradient minimization of the parametric functional (15) by a factor of two. The behavior of the misfit functional is a good indicator to measure the efficiency of the inversion process. Figure 3 shows that the normalized misfit can be reduced to as low as 3% in this case, which corresponds to the level of noise in the data. The corresponding quasi-optimal value of the regularization parameter for the final iteration was $\alpha_{qo} = 0.05$. The CPU time for numerical calculations using QL inversion was 120 minutes.

Let us look at the most important result of the inversion: the resistivity distribution. Figure 4 shows the 3-D inversion image of the predicted model by inversion carried out using TE and TM data simultaneously. One can clearly see in this figure the configuration of the conductive synclinal structure.

Figure 2 shows the comparison between synthetic observed data and predicted data for the inversion result presented in Figure 4. One can see that predicted data based on QL approximation fit very well the initial (synthetic observed) data because the inversion was based on the QL method. At the same time, there is a small discrepancy between predicted data based on the IE method and the initial (synthetic observed) data. This discrepancy reflects actually the level of QL approximation accuracy in the forward modeling solution. It demonstrates also the practical limitations of QL inversion: this inversion can be used for geoelectrical models with relatively small conductivity contrasts between different geoelectrical structures. According to Zhdanov and Fang (1996a), QL approximate forward modeling is valid for a conductivity contrast up to 100. Thus, we should conclude that QL inversion works well only within the limits of QL approximation.

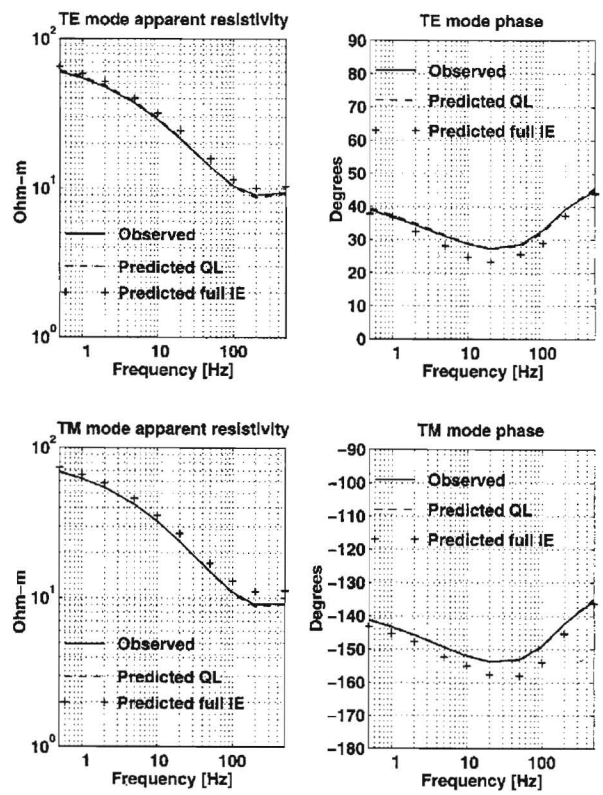

FIG. 2. Typical magnetotelluric sounding curves at $x = 0$, $y = 90$ m above the initial and predicted model for the synthetic data inversion. We plot three curves for each mode: (1) initial synthetic observed data computed using the IE method (solid lines), (2) predicted data computed for inverse model using QL approximation (dashed lines), and (3) predicted data computed for inverse model using the IE method (lines formed by crosses).

In summary, numerical modeling and inversion results demonstrate that QL inversion can produce reasonable images of 3-D geoelectrical structures. We will discuss below the two case histories of interpreting MT and CSAMT data using QL inversion.

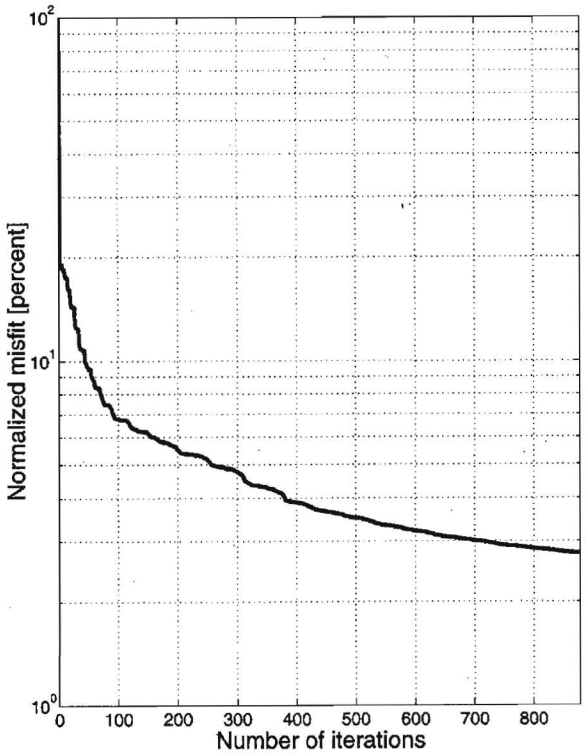

FIG. 3. Behavior of the misfit functional during the inversion for the synthetic data contaminated by 3% noise.

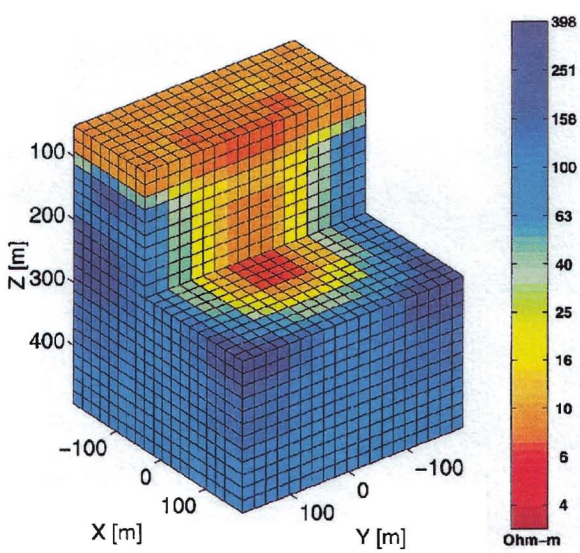

FIG. 4. Volume image of the inversion result for the synthetic model.

CASE STUDY IN THE MINAMIKAYABE AREA, JAPAN

The New Energy and Industrial Technology Development Organization (NEDO) has been conducting a "Geothermal Development Promotion Survey" in the Minamikayabe area located in the southern part of Hokkaido, Japan (Takasugi et al., 1992). This area is particularly interesting because of its geothermal potential. In 1988, MT sounding and AMT sounding were conducted in this area. Figure 5 shows the location of the MT measurement sites. The site spacing is 100 m along and across observational profiles (Figure 5). The frequency range of MT data is from 1 to 130 Hz. Because the survey area at Minamikayabe is located very close to Uchiura Bay on the northeastern side, low frequency data are strongly affected by the "coast effect" (Takasugi et al., 1992). Since we are interested in the shallow geological structure in this area, it is reasonable to restrict ourselves to frequencies which are greater than 1 Hz so that the coast effect can be neglected. We use MT data for inversion at seven different frequencies between 1 and 100 Hz (96, 48, 24, 12, 6, 3, and 1.5 Hz). In order to reasonably choose the background model for the inversion, we first apply one-dimensional inversion to all observed data and approximate the background model as a three-layer model (the resistivities are 480, 6, and 150 ohm-m; the thicknesses are 30 and 450 m).

We use both nominal TE mode and TM mode data for a total of 161 MT soundings in the inversion. In this area, we expect to find a geothermal high conductivity zone in the intrusive resistive rock. This assumption is reflected in our three-layer background model. The subdivisions of the inverse area are shown in Figure 6. It was divided into 16×16 cells in a horizontal

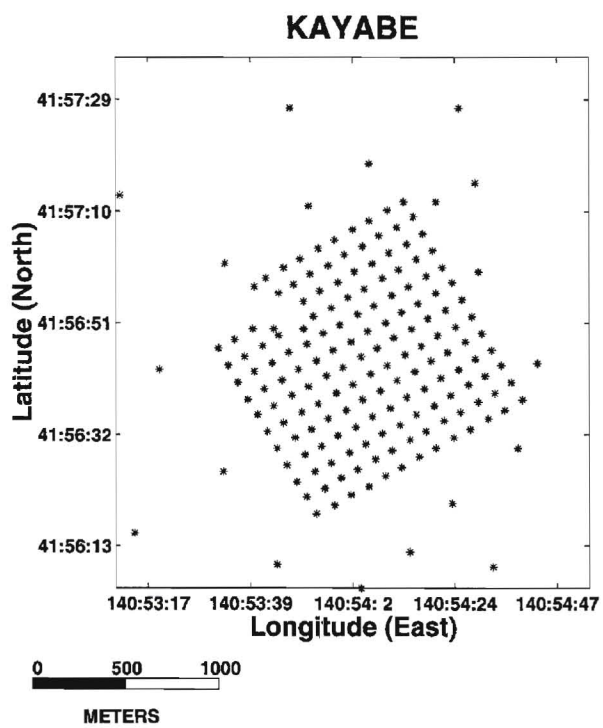

FIG. 5. The distribution of MT sounding sites in the Minamikayabe area. Stars denote the positions of MT sites.

plane (each cell has is 100 m × 100 m size) and seven layers in a vertical direction. This is consistent with the spacing of 100 m between the observational points.

After 320 iterations of the QL inversion scheme we reached the misfit of 8%. The CPU time for this computing was about 200 minutes. Figures 7 and 8 show the inverse results. Figure 7 presents the general 3-D images of the model, whereas Figure 8 shows vertical slices along three profiles. The 3-D inversion is consistent with the 2-D interpretation results included in Takasugi et al. (1992); that is, there exists a low resistivity area (middle layer) in the intrusive resistive rock formation. As a general tendency, the resistivity varies with depth approximately as high-low-high, and also a resistive zone exists within the low resistivity layer, which is in agreement with the result of Takasugi et al. (1992). However, 3-D inversion produces much more detailed information about the internal structure of the inverse area.

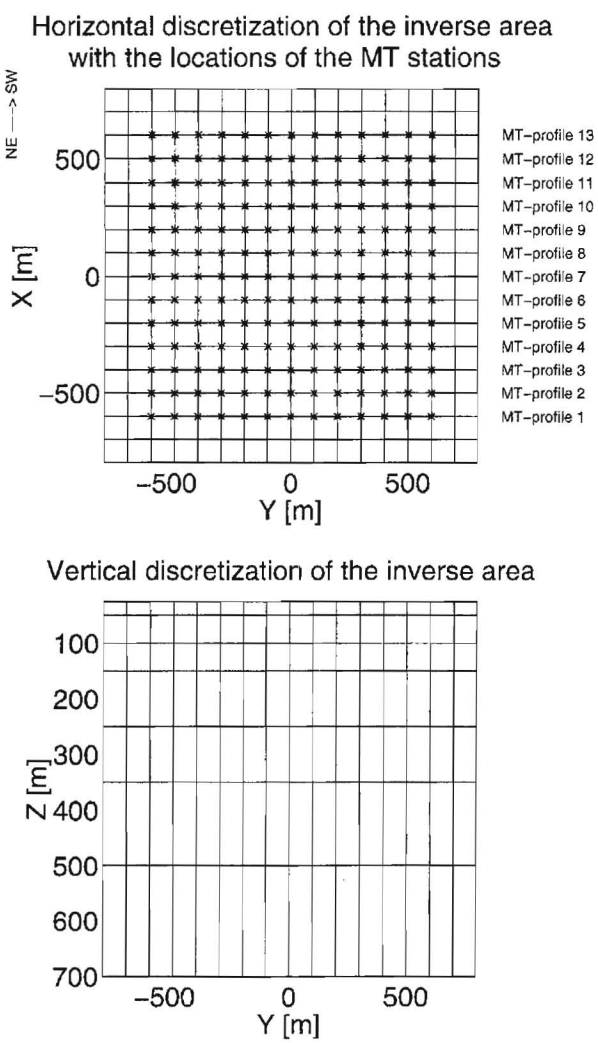

FIG. 6. The subdivision of the inverse area for Japanese MT data (16 × 16 × 7). Top panel is plan view; bottom panel is vertical cross-section. The MT stations are marked by stars on the horizontal cross-section (top panel).

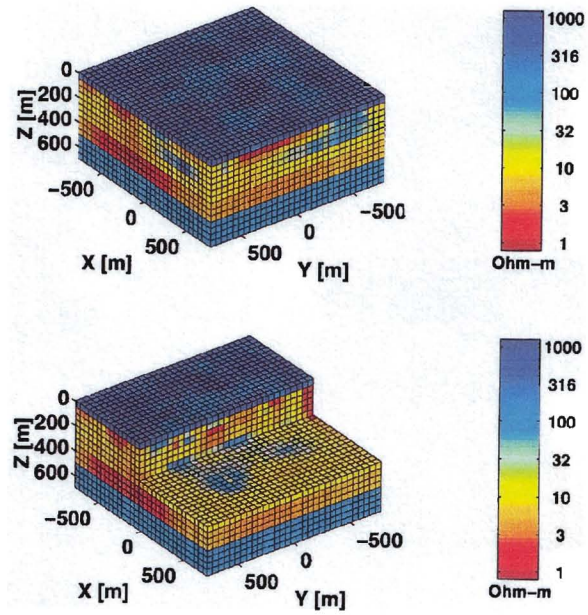

FIG. 7. 3-D resistivity images of the inverse results obtained by QL inversion of the MT data.

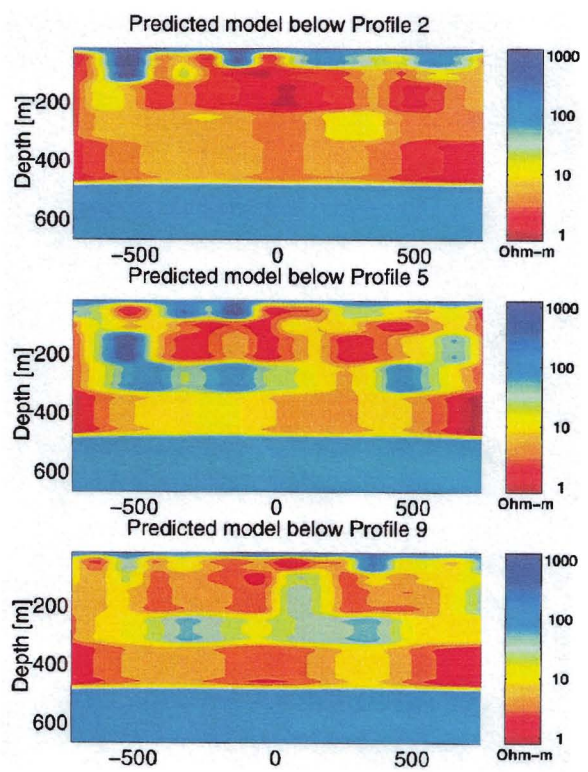

FIG. 8. The vertical slices of the inverse results for the Japanese MT data along Profiles 2, 5, and 9.

The comparisons of original data with the predicted data are presented in Figures 9 and 10. They show good agreement between the observed and predicted apparent resistivity and phase pseudosections.

3-D INVERSION OF TENSOR CSAMT DATA COLLECTED OVER THE SULPHUR SPRINGS THERMAL AREA, VALLES CALDERA, NEW MEXICO, U.S.A.

The Valles Caldera, New Mexico, U.S.A. is one of the Quaternary rhyolite systems of North America. To examine its volcanic history an extensive CSAMT survey was carried out over the Sulphur Springs geothermal area in the caldera (Wannamaker, 1997a, b). The detailed geology of the measured area and the receiver system is shown in Figure 11. Two independent electric bipoles were used as a transmitter at 13-km distance from the measured area. Frequency soundings were carried out along four profiles at 45 receiver points marked in Figure 11 (N1, N2, S1, and E1). The frequency range was 4–4096 Hz.

The tensor CSAMT methodology was based, according to Wannamaker (1997a, b), on measuring five EM field components (E_x, E_y, H_x, H_y, H_z) for two independent polarizations of source current bipoles. Plane-wave impedances and H_z tensor elements were obtained at each frequency. For example, the off-diagonal impedance elements were computed by the formulas:

$$Z_{xy} = \frac{E_{x2}H_{x1} - E_{x1}H_{x2}}{H_{x1}H_{y2} - H_{x2}H_{y1}}, \tag{30}$$

and

$$Z_{yx} = \frac{E_{y2}H_{y1} - E_{y1}H_{y2}}{H_{x1}H_{y2} - H_{x2}H_{y1}}, \tag{31}$$

where subscripts 1 and 2 refer to the source bipole number. Apparent resistivities (ρ_{xy} and ρ_{yx}) and impedance phases (ϕ_{xy} and ϕ_{yx}) were calculated in the usual manner. The quantities ρ_{xy} and ϕ_{xy} were assigned to the nominal TE mode, whereas ρ_{yx} and ϕ_{yx} were assigned to the nominal TM mode. Wannamaker (1997a, b) noted that while this 2-D terminology was only approximate, it still was consistent with the strike directions of the major geological structures beneath the observational lines (Figure 11).

For our 3-D quasi-linear inversion, we were able to use only these quantities, apparent resistivities (ρ_{xy} and ρ_{yx}) and impedance phases (ϕ_{xy} and ϕ_{yx}), because the original EM field components data were not available. At the same time, numerical analysis conducted by Wannamaker (1997a, b) and our own numerical results have demonstrated that nonplane-wave effects associated with the resistive crystalline basement are

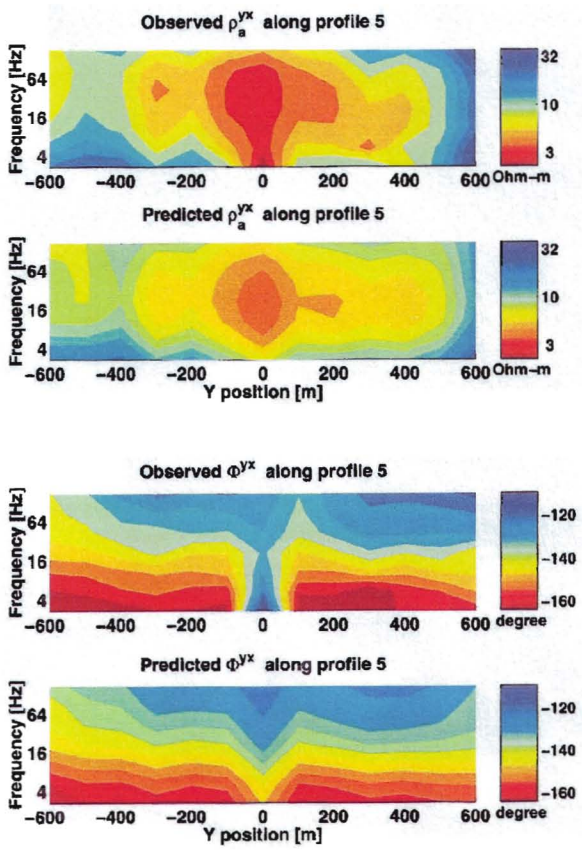

FIG. 9. Comparison of apparent resistivity and phase (TM mode) pseudosections between the observed and predicted data along profile 5.

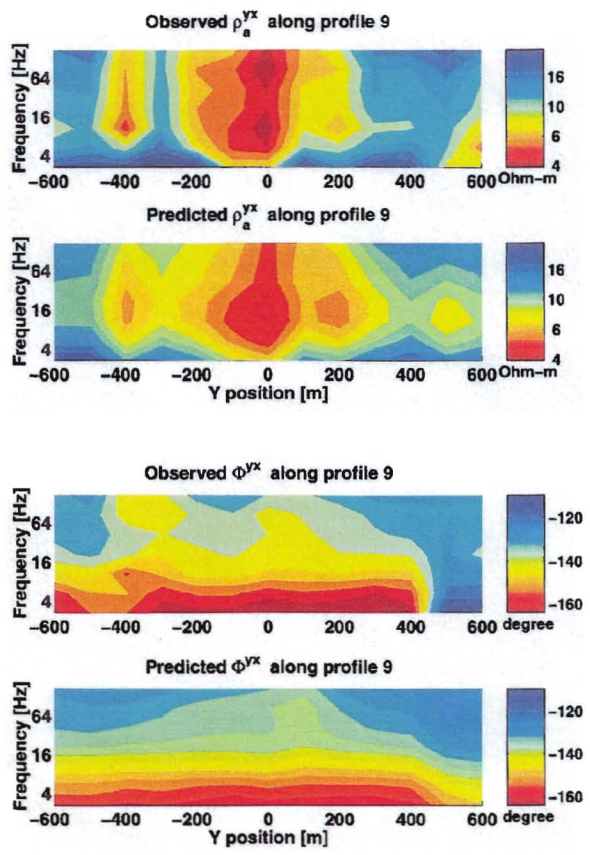

FIG. 10. Comparison of apparent resistivity and phase (TM mode) pseudosections between the observed and predicted data along profile 9.

observed in the CSAMT data at 8 Hz and lower frequencies. In other words, theoretical CSAMT sounding curves, computed using formulas (30) and (31) practically coincide with the theoretical MT soundings curves for the geoelectrical structures typical in the caldera. To demonstrate this fact, we present the results of forward modeling for three 1-D models which can be considered as typical in the caldera.

Models A and B are three-layer models with 12–8–500 ohm-m resistivities and 250–750 m thicknesses, and model C represents a five-layer model with 458–165–7–500–20 ohm-m resistivities and 32–200–750–10 0000 m thicknesses. We calculated theoretical MT and CSAMT apparent resistivity and phase curves versus frequency for these models. Figure 12 presents the ratio of these curves. One can see that down to $f = 8$ Hz, the ratios of the corresponding MT and CSAMT apparent resistivities and phases are equal to one. So, we can state that the observed CSAMT data can be treated as plane-wave data. That is why it was reasonable to interpret this data on the

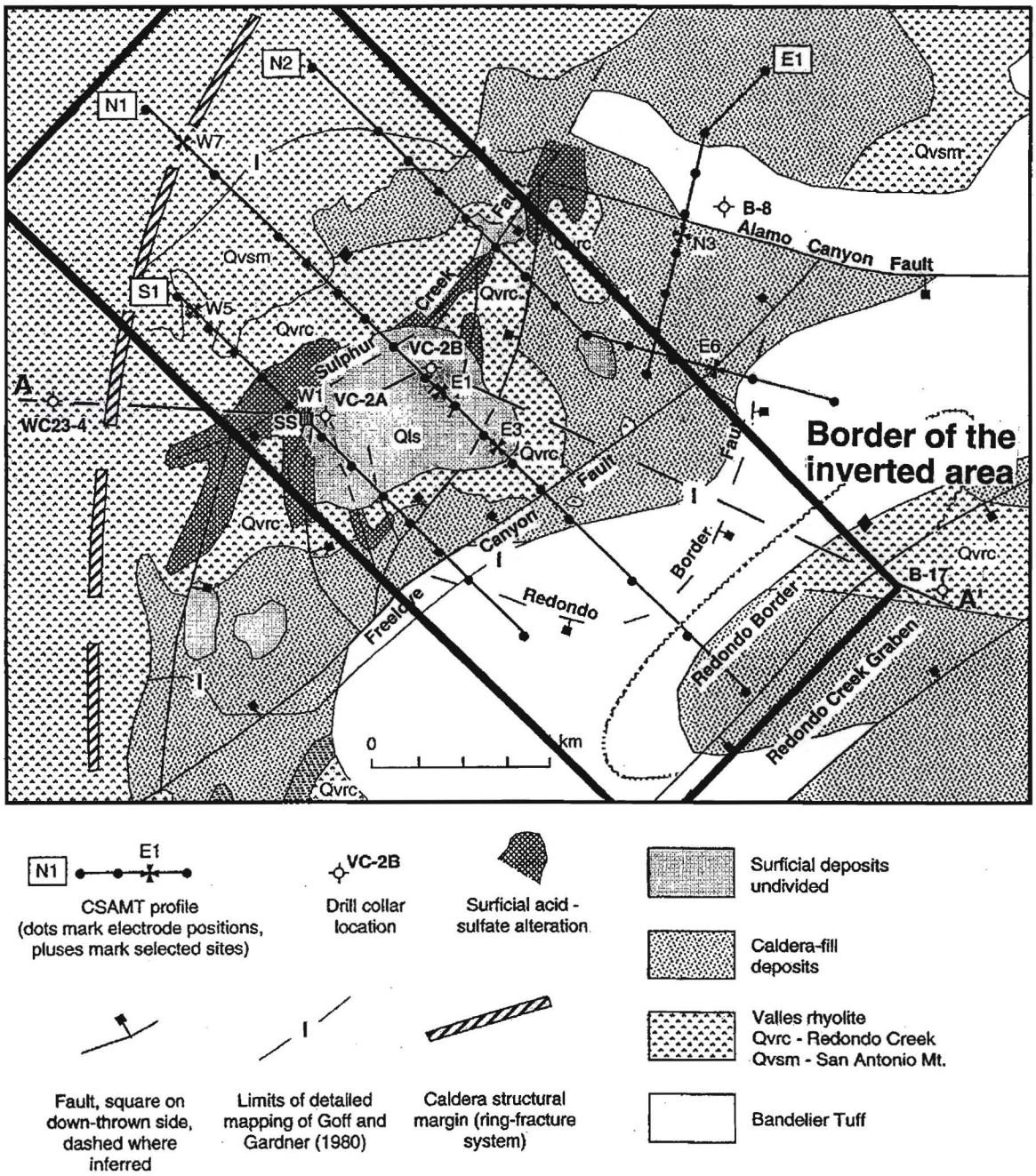

FIG. 11. Detailed geological map of the Sulphur Springs area in the Valles Caldera (after Wannamaker, 1997a) with the receiver profiles and the border of the area used for the inversion shown by thick black lines.

basis of conventional MT formulas in a similar way, as was done for the MT survey in the previous case history. We used for inversion the CSAMT data along three profiles N1, N2, and S1 (Figure 11). Observed frequency sounding TE- and TM-mode CSAMT apparent resistivity and phase pseudosections along the central line (N1) are shown in Figures 13 and 14.

The subdivision of the inverse area in the rectangular cells is shown in Figure 15. We divided the area into 20 by 5 cells in a horizontal plane (see top panel in Figure 15). Each cell is 500 m long in the X direction and 200 m long in the Y direction, which corresponds to the minimum distance of 200 m between the receivers along the observation lines and the distance of 700 m between the profiles. Note also that the length of the electric receiver bipoles is 250 m. Taking into account the spacing of the observational system, it seems unreasonable to select the horizontal size of the inversion grid cells less than 200 m. We used seven different depth levels of the volume grid. The vertical sizes of the substructures increase with depth (bottom panel in Figure 15).

After 500 iterations of the QL inversion scheme which required 150 minutes of CPU time, we reached the misfit of 7%. Figure 16 shows the results of inversion for three vertical slices passing through the observational lines. Figures 13 and 14 represent also the predicted pseudosections for the TE- and TM-mode apparent resistivity and phase along the central line of the survey.

Note that the result of the 3-D inversion is consistent with the previous 2-D inversion results (Wannamaker, 1997a). Figure 17 shows 2-D interpretation result obtained by Phil Wannamaker along the central line. One can see strong correlation between these two results. We can clearly locate the typical geoelectrical layers which correspond to the known geological structures of the area. For example, we observe a resistive Bandelier Tuff in the western part of the cross-section and a low resistive Paleozoic sedimentary rocks below the tuff. Also, we can clearly see in the results of 3-D inversion the conductive structure at the depth of about 600–1000 m which can be associated with the Sulphur Creek fault in the western part of the cross-section (Figure 17).

Note that the 3-D inversion results produce much more detailed information about deep geological structures of the caldera than the 2-D inversion. For example, similar to 2-D results presented in Wannamaker (1997a), we observe the low resistivities of the Bandelier Tuff southeast of Sulfur Creek under all three profiles. However, the downdrop in the Paleozoic rocks along the Redondo Border fault is expressed more strongly in the N1 and N2 profiles, and it is not as clearly seen in the S1 profile (Figure 16). In contrast to the 2-D interpretation, one can clearly see the high-resistive zone in the upper 500 m in the central part (near horizontal coordinates $x = 0$ and $y = 0$) of the 3-D inverse image (Figure 16, middle panel; Figure 18, bottom panel). It may possibly correspond to a vapor zone near the well VC-2B (Figure 11) as implied from acid-sulphate

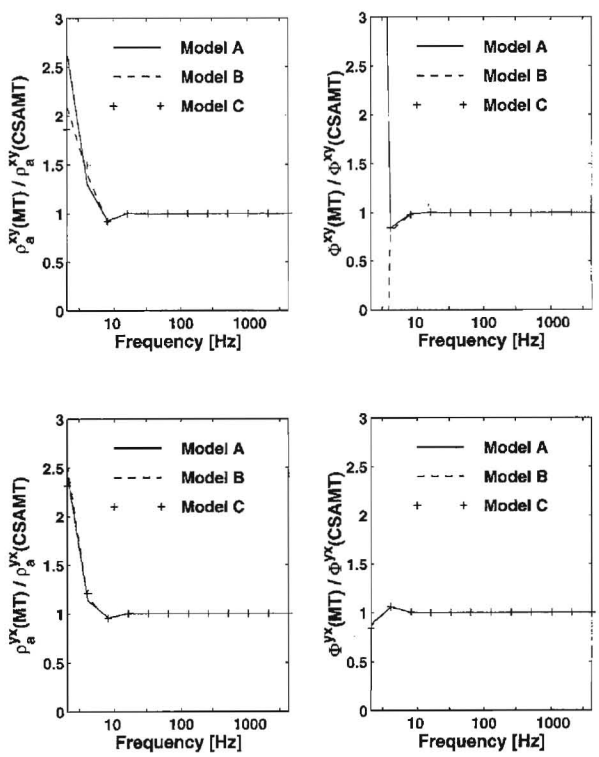

FIG. 12. Ratios between MT and CSAMT apparent resistivities and phases versus frequency for three synthetic models.

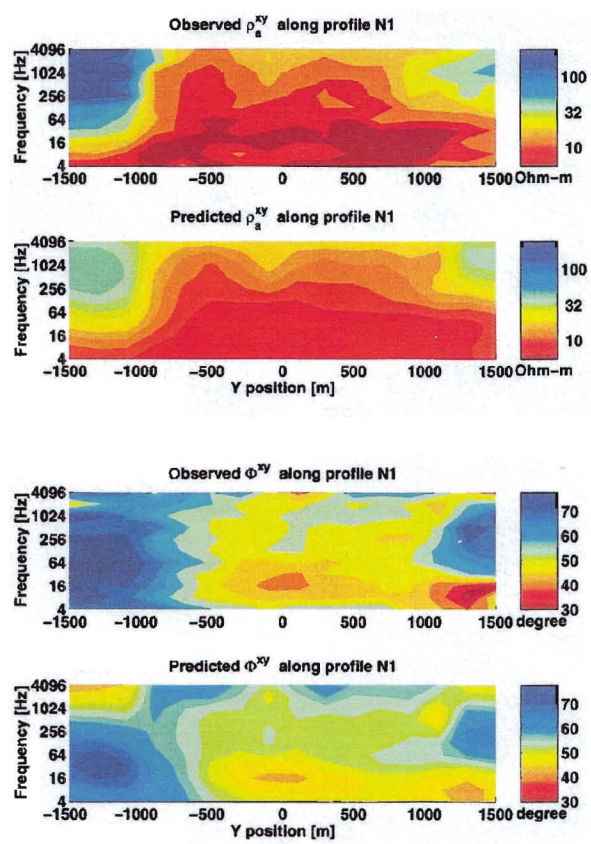

FIG. 13. Observed and predicted TE-mode apparent resistivity and phase pseudosections along the central profile (N1) of the CSAMT survey.

alteration and subhydrostatic well pressures (Wannamaker, 1997a). Note that this zone was not detected by 2-D interpretation of CSAMT data.

CONCLUSION

We have developed a rapid 3-D electromagnetic inversion algorithm based on the QL approximation of the forward modeling. The main advantage of the method is that we reduce the original nonlinear inverse problem to a set of linear inverse problems to obtain a rapid 3-D EM inversion. The QL inverse problem is solved by a regularized conjugate gradient method which ensures stability and rapid convergence. The inversion of the real data indicates that 3-D quasi-linear EM inversion is fast and stable. The inverse results provide reasonable recovery of the models and real geological features. The main limitation of QL inversion is that it can work well only within the limits of QL approximation. Practically, it means that QL inversion can provide an accurate estimate of the geoelectrical model with a conductivity contrast up to 100.

ACKNOWLEDGMENTS

Financial support for this work was provided by the National Science Foundation under grant EAR-9614136. The authors acknowledge the support of the University of Utah Consortium of Electromagnetic Modeling and Inversion (CEMI), which includes Advanced Power Technologies, BHP, INCO, Japan National Oil Corporation, Mindeco, MIM Exploration, Naval Research Laboratory, Newmont, Rio Tinto, Shell International

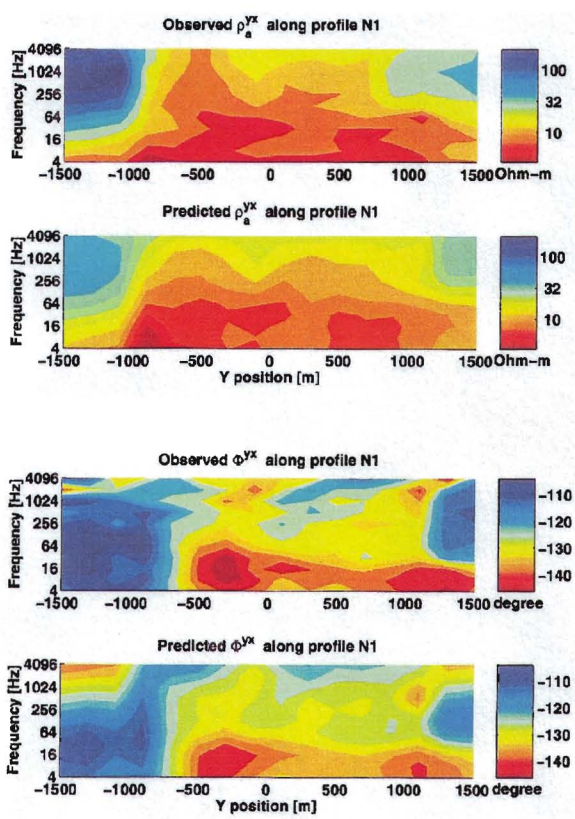

FIG. 14. Observed and predicted TM-mode apparent resistivity and phase pseudosections along the central profile (N1) of the CSAMT survey.

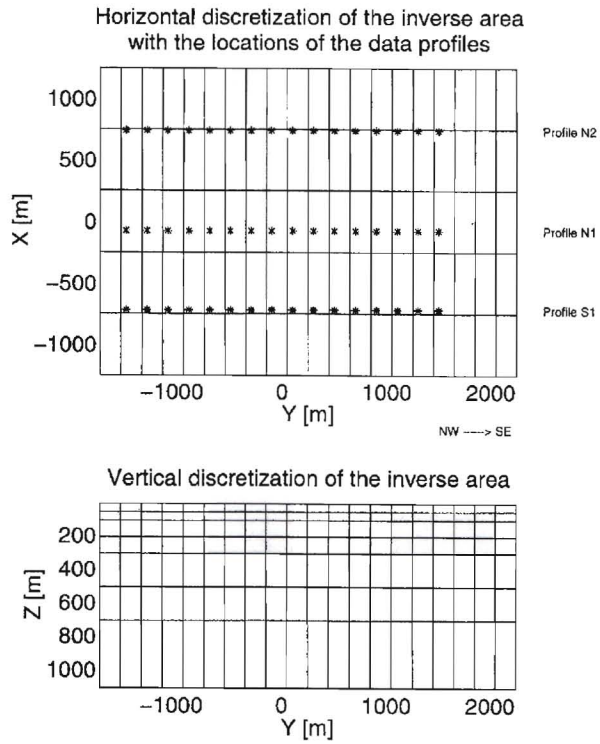

FIG. 15. The subdivision of the inverse area for CSAMT data ($5 \times 20 \times 7$). The locations of CSAMT stations used for the inversion are marked by stars on the horizontal cross-section (top panel). These data are obtained by interpolation to the uniform grid.

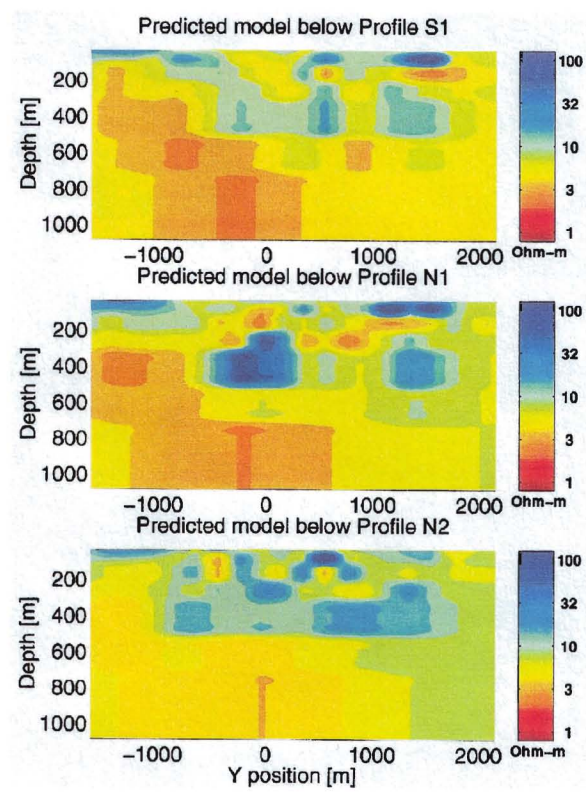

FIG. 16. Vertical cross-sections of the predicted model obtained bv OL inversion of the CSAMT data.

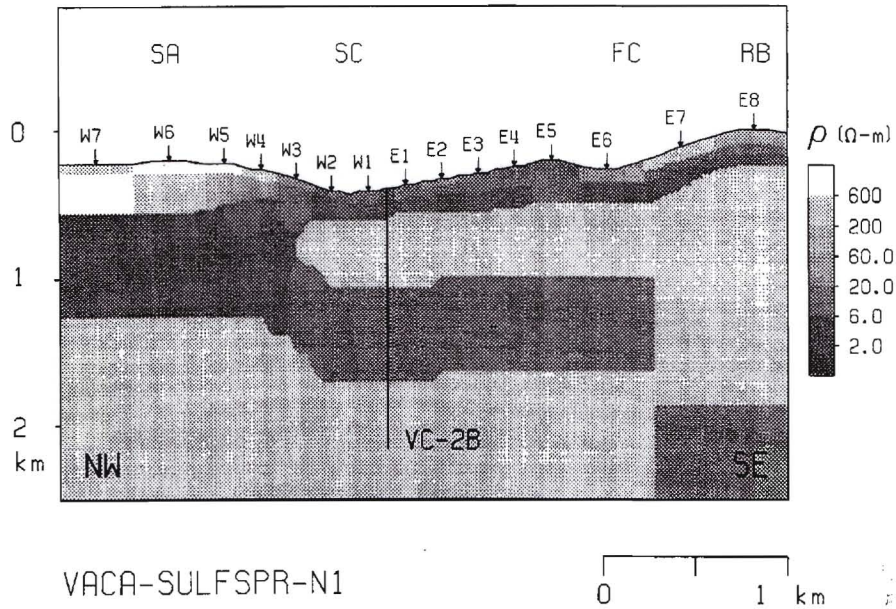

FIG. 17. Result of the 2-D interpretation along the central line of the survey N1 (after Wannamaker, 1997b).

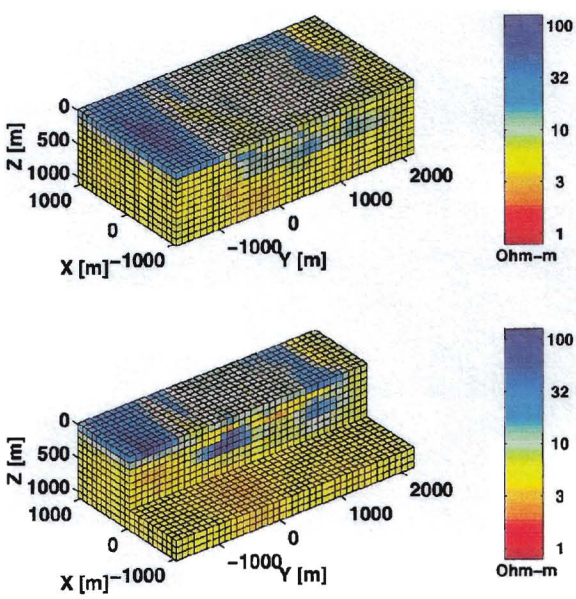

FIG. 18. 3-D resistivity images of the inverse results obtained by QL inversion of the CSAMT data.

Exploration and Production, Schlumberger-Doll Research, Western Atlas, Western Mining, Unocal Geothermal Corporation, and Zonge Engineering.

We are also thankful to Dr. Takasugi, GERD, Japan, for providing the 3-D MT data. We would like to thank Dr. P. Wannamaker for providing us the tensor CSAMT data and useful discussions.

We thank the anonymous reviewers for their useful suggestions and comments.

REFERENCES

Eaton, P. A., 1989, 3-D electromagnetic inversion using integral equations: Geophys. Prosp., **37**, 407–426.

Gusarov, A. L., 1981, About the uniqueness of the solution of the magnetotelluric inverse problem, *in* Mathematical models in geophysical problems: Moscow University Press, 31–80.

Habashy, T. M., Oristaglio, M. L., and de Hoop, A. T., 1994, Simultaneous nonlinear reconstruction of two-dimensional permittivity and conductivity: Radio Sci., **29**, 1101–1118.

Kleinman, R. E., and van den Berg, P. M., 1993, An extended range-modified gradient technique for profile inversion: Radio Sci., **28**, 877–884.

Lee, K. H., and Xie, G., 1993, A new approach to imaging with low frequency EM fields: Geophysics, **58**, 780–796.

Madden, T. R., and Mackie, R. L., 1989, Three dimensional magnetotelluric modeling and inversion: Proc. IEEE, **77**, 318–332.

Nekut, A., 1994, EM ray trace tomography: Geophysics, **59**, 371–377.

Newman, G. A., and Alumbaugh, D. L., 1996, 3-D EM modeling and inversion on massively parallel computers: Sandia Report SAND96-0852.

Oristaglio, M. L., Wang, T., Hohmann, G., and Tripp, A., 1993, Resistivity imaging of transient EM data by conjugate-gradient method: 63rd Ann. Internat. Mtg., Soc. Expl. Geophys., Expanded Abstracts, 347–350.

Pellerin, L., Johnston, J., and Hohmann, G., 1993, 3-D inversion of EM data: 63rd Ann. Internat. Mtg., Soc. Expl. Geophys., Expanded Abstracts, 360–363.

Smith, J. T., and Booker, J. R., 1991, Rapid inversion of two- and three-dimensional magnetotelluric data: J. Geophys. Res., **96**, no. B3, 3905–3922.

Svetov, B. S., and Gubatenko, V. P., 1985, About the equivalence of the system of the extraneous electric and magnetic currents: Radiotechniques and Electronics, no. 4, 31–40.

Takasugi S., Keisaku T., Noriaki K., and Shigeki M., 1992, High spatial resolution of the resistivity structure revealed by a dense network MT measurement—A case study in the Minamikayabe area, Hokkaido, Japan: J. Geomag. Geoelectr., **44**, 289–308.

Tarantola, A., 1987, Inverse problem theory: Elsevier.

Tikhonov, A. N., and Arsenin, V. Y., 1977, Solution of ill-posed problems: W. H. Winston and Sons.

Torres-Verdin, C., and Habashy, T. M., 1995, An overview of the extended Born approximation as a nonlinear scattering approach and its application to cross-well resistivity imaging: Progress in Electromagnetic Research Symposium Proc., 323.

Wannamaker, P., 1997a, Tensor CSAMT survey over the Sulphur Springs thermal area, Valles Caldera, New Mexico, U.S.A., Part I: Implications for structure of the western caldera: Geophysics, **62**, 451–465.

———, 1997b, Tensor CSAMT survey over the Sulphur Springs thermal area, Valles Caldera, New Mexico, U.S.A., Part II: Implications for CSAMT methodology: Geophysics, **62**, 466–476.

Weidelt, P., 1975, EM induction in three-dimensional structures: J. Geophys., **41**, 85–109.

Xie, G., and Lee, K. H., 1995, Nonlinear inversion of 3-D electromagnetic data: Progress in Electromagnetic Research Symposium Proc., 323.

Xiong, Z., 1992, EM modeling of three-dimensional structures by the method of system iteration using integral equations: Geophysics, **57**, 1556–1561.

Zhdanov, M. S., 1993, Regularization in inversion theory, tutorial: Colorado School of Mines.

Zhdanov, M. S, and Chernyak, V. V., 1987, An automated method of solving the two-dimensional inverse problem of electromagnetic induction within the earth: Transaction (Doklady) of the USSR Academy of Sciences, Earth Science Sections, **296**, no. 4–6, 59–63.

Zhdanov, M. S., and Fang, S., 1996a, Quasi-linear approximation in 3-D EM modeling: Geophysics, **61**, 646–665.

———, 1996b, 3-D quasi-linear electromagnetic inversion: Radio Sci., **31**, 741–754.

Zhdanov, M. S., and Keller, G. V., 1994, The geoelectrical methods in geophysical exploration: Elsevier.